CHEMISTRY OF MATERIALS

Subscriber access provided by University of East Anglia Library

Article

Significantly enhanced thermoelectric performance of #-In2Se3 through lithiation via chemical diffusion

Jiaolin Cui, Hua Peng, Zhiliang Song, Zhengliang Du, Yimin Chao, and Gang Chen

Chem. Mater., **Just Accepted Manuscript** • DOI: 10.1021/acs.chemmater.7b02467 • Publication Date (Web): 09 Aug 2017

Significantly enhanced thermoelectric performance of γ-In_2Se_3 through lithiation via chemical diffusion

Jiaolin Cui, [†]* *Hua Peng,* [‡] *Zhiliang Song,* [†] *Zhengliang Du,* [†] *Yimin Chao,* [§]* *Gang Chen* [‡]*

[†] *School of Materials and Chemical Engineering, Ningbo University of Technology, Ningbo 315016, China*

[‡] *School of Physics and Technology, University of Jinan, Jinan, 250022, China*

[§] *School of Chemistry, University of East Anglia, Norwich NR4 7TJ, United Kingdom*

ABSTRACT γ–In_2Se_3 is selected as a thermoelectric candidate because it has a unique crystal structure and thermal stability at relatively high temperatures. In this work we have prepared lithiated γ – In_2Se_3 through chemical diffusion and investigated its band structures and thermoelectric performance. After 30 h lithiation of γ–In_2Se_3 in lithium acetate (CH_3COOLi) solution at 50°C, we have observed a high Hall carrier concentration (n_H) up to 1.71×10^{18} cm^{-3} at room temperature (RT), which is about 4 orders of magnitude compared to that of pristine γ – In_2Se_3. The enhancement in n_H is directly responsible for the remarkable improvement in electrical conductivity, and can be elucidated as the Fermi level (F_r) unpinning and moving towards the conduction band (CB) through the dominant interstitial occupation of Li^+ in the γ – In_2Se_3 lattice. Combined with the minimum lattice thermal conductivity (κ_L=0.30~0.34 $WK^{-1}m^{-1}$) at ~923 K, the highest ZT value of 0.62~0.67 is attained, which is about 9~10 times that of pristine γ – In_2Se_3, proving that the lithiation in γ–In_2Se_3 is an effective approach on the improvement of the thermoelectric performance.

1. Introduction

Thermoelectric (TE) materials have attracted much attention in recent years that they are capable of harvesting huge amount of waste heat by converting heat into electricity. However, the conversion efficiency is still low and high performance TE materials are limited up to date. Although many compounds, such as PbTe – ,[1,2] SnSe–,[3,4] Mg_2Si–[5] and some other tellurides,[6] present potential TE performance, it is still urgent to develop high performance and new environmentally benign TE materials for mid temperature power generation applications.

Indium selenide (In_2Se_3) could be used as phase – change random access memory device and thermoelectric material, due to its large bandgap,[7] intrinsic low thermal conductivity and high Seebeck coefficient.[8 – 10] However, there are different coexisting phases and crystal structures, such as rhombohedral / hexagonal α / β phases, hexagonal γ and δ phases, some of which, for example, α– and β – phases, exist in a metastable state and are inclined to mutual transformation on heating or cooling.[11] Therefore, it is difficult to synthesize single α– or β–In_2Se_3–based solid solutions.[12,13] Accordingly, the γ–phase, which is stable above 520 C°,[12] 625 C° [14] or 650 C°,[15] in terms of different experiments, might be an alternative indium selenide used for TE applications in the region of mid to high temperatures.

γ – In_2Se_3 behaves like an insulator with the bandgap of 1.9 eV.[16] Unlike α–In_2Se_3, it has intrinsic screw – like ordering vacancies,[17 – 19] instead of layer – like ones. However, there are 1/3 structural

vacancies existing along the c–axis in γ–In_2Se_3, which accommodates cations with different sizes. It has been reported that the diffusion of cations, such as Li with small size, into the crystal lattice of In_2Se_3, forms metallic phase $Li_{0.1}In_2Se_3$, enhancing the free carrier concentration by more than three orders of magnitude (from 10^{16} cm^{-3} to 1.5×10^{19} cm^{-3}).[20] In addition, the impurity occupation in the cation sites could induce the shift of the Fermi level (F_r), thus engineering the band structure.[21] Therefore, the impurity doping in γ–In_2Se_3 have a profound impact on the structure and TE performance of the host materials.

In this work, we have prepared lithiated γ–In_2Se_3 powders via chemical diffusion, and examined transport and TE properties from room temperature (RT) to ~930 K. The experiments reveal that doping of Li ion in γ–In_2Se_3 enhances the Hall carrier concentration (n_H) by about 4 orders of magnitude, and thereby significantly improves the TE performance with the highest ZT value of 0.62~0.67 at ~923 K. This value is 9~10 times that of pristine γ–In_2Se_3, proving that lithiation in γ–In_2Se_3 is playing a great role to improve the TE performance.

2. Experimental

Sample preparations Two elemental powders of In and Se with the purity of more than 99.999% were loaded into the vacuum silica tube, according to the stoichiometry In_2Se_3, and melted at 1273 K for 10 h followed by cooling to 950 K and holding at this temperature for 168 h, then cooled to RT rapidly. The as–solidified ingots were pulverized in agate mortar and then ball milled in stainless-steel bowls containing benzinum at a rotation rate of 350 rpm for 10 h. A pure γ–In_2Se_3 powder was obtained using above technologies.

Prior to lithiation via chemical diffusion, the powder of γ–In_2Se_3 was sorted by using 200 mesh, thus allowing the powder with the size of ~20 μm to be obtained. Subsequently, the sorted powder was soaked in the lithium acetate (CH_3COOLi) solution for Li diffusion. Owing to the large chemical diffusivity (D) of Li ($D = 10^{-13}cm^2s^{-1}$ to $5.5\times10^{-10}cm^2s^{-1}$) in the In_2Se_3 solution,[22] the Li concentration could be easily get saturated. We therefore determine that the longest lithiation time is 40 h at a fixed temperature of 50 C°. Another diffusion practice was to vary lithiation temperature from 30 C° to 60 C° for a fixed lithiation time of 30 h. After different lithiation processes, the lithiated powders were cleaned using alcohol for several times prior to drying.

The dried powders were directly sintered using a spark plasma sintering apparatus (SPS–1030) under a pressure of 55 MPa and at the highest temperature of 950 K. The total sintering time was less than 2 min, including holding time (30 s) at this temperature. After sintering, the sample was cooled to RT rapidly. Such a rapid sintering procedure could avoid the phase transition caused by the interdiffusion of elements.[13,23,24] After sintering, the consolidated samples were annealed at 950 K for 72 h once more to ensure the pure γ–In_2Se_3 to be obtained. The density (d) of the sintered samples, measured using Archimedes' method, is ~5.34×10^3 kgm^{-3}, which is about 95% theoretical one.[18] Two types of samples were prepared: parallel ($C_{//}$) and perpendicular ($C_{\perp}$) to the pressing directions. They were all cut into 3 mm slices in width from the cylindrical- (ϕ~13.0×14.0 mm^2) and coin-shaped (ϕ 20×3.0 mm^2) bulks, and then polished to be 2.5×12 mm^2 for electrical property measurements. The samples with ϕ 10.0×2.0 mm^2 in $C_{//}$ and $C_{\perp}$ were prepared for thermal diffusivity and heat capacity measurements.

Structural analyses and calculation The powder X–ray diffraction (XRD) patterns were obtained on a Bruker D8 Advance instrument with Cu Kα radiation (λ=0.15406 nm) with a scanning step size of 0.02°.

In order to gain a deep understanding of the crystal structure, the microstructure of lithiated γ–In_2Se_3 sample (lithiation time 30 h at 50 C°) was examined by using high resolution transmission

electron microscopy (HRTEM) (JEM−2010F, 220 kV). Besides, electron energy loss spectroscopy (EELS) data were acquired using a Gatan Model 776 Enfina spectrometer coupled to the JEM−2010F.

The band structures and formation energies upon Li occupation at different lattice sites were calculated using first principle calculation. During calculations, the DFT calculation were carried out within the framework of the plane−wave projector augmented wave formalism as implemented in the Vienna ab−initio Simulation Package (VASP).[25] The generalized gradient approximation (GGA) to the exchange-correlation potential in the Perdew Burke Ernzerhof (PBE) form was used.[26] A plane−wave cutoff energy of 500 eV was used. Brillouin zone sampling scheme of Monkhorts−Pack k−mesh with 6×6×2 was used to generate the k points for calculations. The ground−state structure was obtained to a maximal force on each ion of less than 0.01 eV/Å and the total energy change of less than 1×10^{-6} eV. A supercell consisting of 2×2×1 unit cells of γ−In_2Se_3 were used for defect calculations. The $1s^22s^1$, $5s^25p^1$, and $4s^24p^4$ were treated as valence states of Li, In and Se, respectively.

Measurements of physical properties Hall carrier concentrations (n_H) were determined using Hall coefficient (R_H) at RT measured using a PPMS system. Four−contact Hall−bar geometry (2×2×7 mm^3) was used for the measurement. The n_H and μ values were estimated according to the formula $n_H = 1/eR_H$ and $\mu=|R_H|\sigma$ respectively, where e is the electronic charge.

Electrical conductivities (σ) and Seebeck coefficients (α) were measured simultaneously under He atmosphere from RT to 930 K on a ULVAC−RIKO ZEM−3 instrument system with the uncertainty each < 6%. The thermal diffusivity (λ) and heat capacity (C_p) were measured by the TC−1200RH at RT~930 K with the uncertainty less than 10% respectively. The thermal conductivities (κ) were calculated from $\kappa = dC_p\lambda$, here d is the material density. The lattice contributions (κ_L) were attained from the total κ minus the electronic part κ_e. κ_e is estimated by the Wiedemann−Franz (W−F) relation, $\kappa_e = L_0\sigma T$, where L_0 is the Lorenz constant estimated according to the expression, $L_0=[1.5+\exp(-|\alpha|/116)]\times10^{-8}$ $W\Omega K^{-2}$. [27]

The above data obtained were repeated several times using different samples, and the average data for each parameter was attained. The total uncertainty for ZT was ~22%. In addition, in order to check the thermal stability of the γ−In_2Se_3 after lithiation, we have specially measured the TE properties from high temperature (930 K) to RT (cooling cycle) of the sample ($C_{//}$) with the lithiation time of 30 h at 50 C°.

3. Results and discussions

Structural analyses Fig.S1 shows the X−ray diffraction patterns for the lithiated powders with different soaking times (Fig.S1a) and temperatures (Fig.S1b). All diffraction peaks in the patterns are identical to those of γ−In_2Se_3 phase (PDF: 40−1407: hexagonal crystal structure and space group $P6_1$) with no visible impurity phases identified, indicating that the main phase is γ−In_2Se_3.

To characterize the microstructures and chemical compositions of lithiated γ−In_2Se_3 powders, we have carried out EDS, high−resolution TEM (HRTEM), and electron diffraction (ED) studies. Fig.S2a shows the low−magnification TEM image of a lithiated γ−In_2Se_3 powder for 30 h lithiation at a fixed temperature of 50 C°, in which a typical polycrystalline structure is presented. Fig.S2b is its HRTEM image, inset in Fig.S2b is an enlarged image, where the crystal planes (113) and (110), corresponding to the periodic spacing of 0.31 nm and 0.36 nm in γ−In_2Se_3, are represented respectively. Fig.1 is an electron diffraction (SAED) pattern from a selected area, which matches well with the lattice structure in Fig.S2b, confirming the structure of γ−In_2Se_3. Inset in Fig.1 is the EDS spectrum, where only In and Se elements are identified without Li signal. It is likely that Li element is too small (light) to be detected. The Cu peaks in the spectrum come from Cu grid.

Besides, EDS reveals that the lithiated γ – In_2Se_3 powder has a Se/In atomic ratio of ~1.51, proving the structure and composition of γ–In_2Se_3.

Although Li can penetrate into most materials, its atomic size is too small to be identified using EDS spectrum. Therefore, Electron Energy Loss Spectroscopy (EELS) is used to characterize the change in chemical composition in the current lithiated γ – In_2Se_3 powders. The EELS from the pristine γ–In_2Se_3 and that for 30 h lithiation at 50 C° are shown in Fig.2. Before lithiation, the EEL spectrum reveals only a small peak centered around 56 eV, which should be assigned to the Se core level (Fig.2a), and inset in Fig.2a is its TEM image. Fig.2b is its corresponding line spectrum with background subtracted. However, after 30 h lithiation at 50 C°, a large peak around 56 eV can be clearly observed, as shown in Fig.2c, which is assigned to the core levels of Li K–edge structure mixed with Se, indicating the presence of Li in this material. An inset in Fig.2c is its TEM image. Fig.2d is its corresponding line spectrum with background subtracted. However, the onset of the Li peak position (54 eV) is a little lower than that reported (58 eV) in ref. [17], which might be due to different crystal structure or space group of studied In_2Se_3.

Upon Li occupation in the lattice of γ – In_2Se_3, some changes of the lattice constants of the crystal have been taken place. The lattice constants *a* and *c* as a function of lithiation time (at 50 C°) or lithiation temperature (for 30 h), determined from the refinement of the X-ray patterns using Jade software, are shown in Fig.3a and Fig.3b respectively. The *a* (7.056~7.090 Å) and *c* (19.30~19.35 Å) values for the pristine γ – In_2Se_3, which are in almost agreement with the results reported,[12,18,19,28] increase with lithiation time until 30 h is reached (Fig.3a). Similarly, the average *a* and *c* values increase with lithiation temperature until 50 C° is reached (Fig.3b). Combining with the above results, we believe that Li concentration gets saturated for the lithiation time 30 h at 50 C°. Higher lithiation temperature than 50 C° or longer lithiation time than 30 h gives rise to possible release of Li ion from the material, thus shrinking the lattice structure.

The variations in lattice constants *a* and *c* can be directly confirmed by taking a close look at the peak position shifts in the XRD patterns (see enlarged patterns in Fig.S1), where the main peak positions (110, 006, 300) move toward lower 2θ values with the lithiation time or temperature increasing until 30 h or 50 C° is reached. While the peak position moves toward higher angle as the lithiation time or temperature is increased to 40 h or 60 C°.

Transport properties In order to probe the effect of Li diffusion into the crystal lattice, we have measured the Hall coefficients (R_H) at RT and then calculated the Hall carrier concentration (n_H) and mobility (μ). The results are shown in Fig.4. The n_H and μ values as a function of lithiation time are shown in Fig.4a, where we observed that the mean n_H value increases rapidly from 3.64×10^{14} cm^{-3} (pristine γ–In_2Se_3) to 1.71×10^{18} cm^{-3} (30 h lithiation), ~4 orders of magnitude of initial value, and then deceases to 6.30×10^{16} cm^{-3} (40 h). While the μ value decreases gradually from 26.57 $cm^2v^{-1}s^{-1}$ to the minimum value 2.04 $cm^2v^{-1}s^{-1}$ (30 h), and then increases to 5.28 $cm^2v^{-1}s^{-1}$ (40 h). A similar lithiation temperature dependences of n_H and μ are observed, see Fig.4b. The n_H value increases with lithiation temperature increasing until 50 C° is reached, while the μ value decreases to the minimum at 50 C°. Therefore, it is concluded that the lithiated γ–In_2Se_3 sample for a lithiation time of 30 h at 50 C° gives the highest Hall carrier concentration and lowest mobility. The results coincide well with the variation of the lattice constants, i.e., the higher the Hall carrier concentration after lithiation, the larger the unit cell.

TE performance Since lithiation in γ–In_2Se_3 gives rise to a significant enhancement in Hall carrier concentration, a remarkable improvement in electrical conductivity[29,30] and TE performance are anticipated.

Fig.5a is the Seebeck coefficients (α) perpendicular to the pressing direction ($C_\perp$) as a function of lithiation temperature for the fixed lithiation time of 30 h. The α values are negative, indicating n – type semiconducting behavior. Generally, the absolute α value ($|\alpha|$) decreases with lithiation temperature increasing below the measuring temperature 830 K until the lithiation temperature 50 C° is reached. Above 830 K the $|\alpha|$ value gradually converges, and at 923 K it reaches 180.0~210.0 μVK^{-1} for the lithiated samples. The electrical conductivity (σ), shown in Fig.5b, increases with lithiation temperature increasing until the lithiation temperature 50 C° is reached. The highest σ value is 1.08×10^4 $\Omega^{-1}m^{-1}$ (lithiation 30 h at 50 C°) at the measuring temperature 923 K. This value is about 39 times that of pristine γ – In_2Se_3, which suggests that the lithiation in γ–In_2Se_3 is an effective way to improve the electrical conductivity. Combined with the carrier concentrations shown in Fig.4, the n_H and σ values reach the highest simultaneously among the samples when the lithiation temperature and time are at 50 C° and 30 h.

Fig.5c presents the lattice thermal conductivity (κ_L) against lithiation temperature for a fixed lithiation time of 30 h. Most samples have relatively constant κ_L values at high measuring temperatures, except for the sample with lithiation at 60 C°, which decreases with measuring temperature increasing. The reason is unclear. With the lithiation temperature increasing to 50 C°, the sample gives the lowest κ_L values below 370 K and at 923 K its κ_L value is 0.34 $WK^{-1}m^{-1}$. Inset in Fig.5c is the total thermal conductivities (κ), which bear a resemblance to the κ_L. An exception is that the κ values for most samples increase with temperature increasing at high temperatures. We believe that the increased κ values at high temperatures should not come from the contribution of bipolar effect,[31] because it is usually difficult to observe the bipolar effect in the wide gap semiconductors, like γ – In_2Se_3 with E_g>1.0 eV from calculation and 1.9 eV reported.[16] In this regard, we speculate that there is an another contribution in the γ – In_2Se_3 – based solid solutions. Since the linear lattice thermal conductivity – l/T relation is expected to hold only for temperatures above the Debye characteristic temperature, θ_D, therefore, the constant κ_L values for most samples at high temperatures might involve the contribution of photon conduction, κ_p, described below,[32] although the photon conduction may usually be seen in some polycrystalline oxides, such as BaO and SrO,[33] Al_2O_3 and BeO,[34] and in single crystals of Al_2O_3, MgO, CaF_2 and TiO_2.[35]

$$\kappa_p = 16/3\ \sigma r^2\ T^3\ l_R \qquad (1)$$

here r is the refractive index in the medium, l_R the mean free path of photons. The κ_p value is proportional to T^3. Alternatively, the κ values might involve the contribution of peripheral phonons,[36-37] which increases with the measuring temperature increasing, especially, when the donor levels merge with the conduction band[36-37] (see the electronic structure calculation results below). The third possibility might be the diminution of the structural deformation upon interstitial occupation of Li, which gives rise to less perturbation to the transport of most high – frequency phonons.[38] Anyhow, the abnormal increasing of the total thermal conductivity (κ) at high temperatures requires further investigations.

Combined with the three physical parameters (α, σ, κ), the dimensionless TE figure of merit (ZT) ($C_\perp$) can be obtained. As expected, the ZT value increases with lithiation temperature increasing until the lithiation temperature 50 C° is reached (Fig.5d). The highest ZT value is 0.67 at ~923 K. This ZT value is about 10 times that of pristine γ – In_2Se_3. Although the ZT value is still much lower than those of the state–of–the–art binary selenides reported (such as SnSe: ZT=2.6 at 923 K;[4] In_4Se_3: ZT=1.48 at 705 K [39]), it is worth noting that the ZT value of pristine γ–In_2Se_3 is only ~0.064 at ~923 K, indicating that a

big improvement has been achieved after lithiation. This finding also implies that lithiation in the materials with intrinsic vacancies is an effective approach on the improvement of TE performance, even if the pristine materials behave like insulators.

The TE performance of lithiated γ−In_2Se_3 ($C_\perp$) for different lithiation times (≤ 40 h) at a fixed lithiation temperature of 50 C° is shown in the Fig.6. With the lithiation time increasing, the absolute Seebeck coefficient gradually decreases (Fig.6a), while the electrical conductivity increases (Fig.6b). Similarly, the sample with the lithiation time of 30 h gives relatively low lattice contribution (κ_L) (Fig.6c) and total thermal conductivities (κ) (inset in Fig.6c) at high temperatures. Accordingly, the sample with 30 h of lithiation at 50 C° possesses the highest ZT value in this set of samples (Fig.6d). Besides, the sample with lithiation time of 40 h has an increased κ values at high temperatures.

The TE performance parallel to the pressing direction ($C_{//}$) at a fixed lithiation temperature (50 C°) or time (30 h) are presented in Fig.S3. The results bear resemblance to those of the samples ($C_\perp$). Likewise, the lithiated sample ($C_{//}$, 30 h at 50 C°) gives the highest electrical ($1.11\times10^4\ \Omega^{-1}m^{-1}$), lowest lattice thermal conductivity (0.30 $WK^{-1}m^{-1}$), and highest ZT value (0.62) at ~923 K, about 9 times that of the pristine γ–In_2Se_3.

As stated above, In_2Se_3 has multiple phases in the temperature range from RT to 1150 K,[19,40] each of which is stable in its own existing temperature range. However, the mutual transformation between them easily occurs as the temperature elevates or drops, therefore, it is necessary to check the stability of γ − In_2Se_3, especially, the stability of Li ion in the γ − In_2Se_3 matrix. In this work a cooling cycle measurement of the TE properties has been specially conducted for the sample ($C_{//}$) (lithiation for 30 h at 50 C°). The results are shown in Fig.7, where we observed that there is no big change of the electrical conductivities and absolute Seebeck coefficients between the heating and cooling cycles (Fig.7a and b), but the thermal conductivities (κ) are a little higher than those from the heating cycle (Fig.7c), an inset in Fig.7c is the lattice contribution κ_L. The resultant ZT values in the cooling cycle are about ~20 % lower than those in the heating one above 810 K (Fig.7d). The degradation in TE performance could not be attributed to the release of the Li ions or the reduction of the carrier concentration, because only a limited change of the electrical properties (σ, α) has been taken place, nor could it be due to the change of the chemical compositions, since the ratio of Se/In keeps ~1.5 after cooling cycle, determined by EDAX analysis (see Fig.S4). The possible reason might be due to the decreased phonon scattering (see inset in Fig.7c) caused by the increased crystallinity after cooling cycle (see the XRD analysis in Fig.S5) if compared with that of as-solidified ingot. Besides, no visible impurity phases and phase changes were identified after cooling cycle, according to Fig.S5.

Lithiation via chemical or electrochemical route has been extensively applied in α−In_2Se_3 to improve the electrical conductivity of microbatteries,[20,41,42] because the α − In_2Se_3 has a layer − like crystal structure. The bonding inside the layers of α−In_2Se_3 is strongly covalent, while the interlayer interaction (Se−Se) is of the Van der Waals type. Therefore, Li is easily intercalated into the Van der Waals gap. Although γ − In_2Se_3 does not have a layer − like structure, it is of ordered vacancies in screw form (VOSF).[17,19,43,44] These vacancies are still capable of accommodating foreign impurities, such as Li^+ through diffusion, which expands the unit cell. That is the reason why we have observed the increasing of the lattice constants *a* and *c* (Fig.3).

On the other hand, the ion transport in mixed electronic and ionic conductors proceeds through the simultaneous movement of electrons. If the requirement of local electrical neutrality is taken into consideration, one condition should be set for a monovalent ion as Li^+, that is: the diffusion flux of

Li^+ (J_{Li+}) should be equal to that of electrons (J_{e-}) upon equilibrium,

$$J_{Li+} = J_{e-} \quad (2)$$

This suggests that the charge transferring between guest species and host structure are lithiation temperature and time dependent. This explains why the highest carrier concentration has observed under the specific lithiation condition (Fig.4).

In order to further elucidate the origin of the carrier concentration enhancement caused by the Li^+ insertion into the γ – In_2Se_3, we have specially calculated the band structures using the first principle calculation. Fig.8a is showing the band structure and corresponding density of states (DOS) of γ–In_2Se_3, where the Fermi level (F_r) is located on the edge of valence band maximum (VBM). The electron transport properties are determined by the states near the conduction band minimum (CBM), which are coming from the strong coupling of the In – s and Se – p states, while the hole transport properties are mainly governed by the states near the VBM which are mainly from Se–p state. Fig.8b shows the 3D electron localization function (ELF) isosurfaces maps of γ – In_2Se_3 for ELF=0.8 and ELF=0.9, which show a lobe–shaped asymmetrically localized electron cloud around Se^{2-}, indicating the degree of electron localization. Since there are lone–pair electrons surrounding Se atoms from the maps along with the activity of the Se–p state near the VBM, we therefore presume that the pristine γ–In_2Se_3 should have a low electrical conductivity. This calculation is in agreement with the experimental results, as shown in Fig.5b and 6b.

Fig.9 presents the formation energies (E_f) of defects as a function of the Fermi energy (F_r) under the Se–rich and Se–poor conditions, based on the relationships below:

$$E_f = E_{tot}[\text{defect}] - E_{tot}[\text{ref}] - \mu[\text{Li}] + \mu[\text{In or Se}] + q(E_f + E_v + \Delta V) \quad (3)$$

$$\mu[\text{Se}]_{min} = (E[In_2Se_3] - 2\mu[\text{In}]_{bulk}) / 3 \quad (4)$$

here E_{tot}[ref] denotes the total energy of the perfect–crystal supercell, μ[Li] chemical potential of Li^+, q : charge state, E_v valence band maximum in the bulk, ΔV alignment of the average electrostatic potential in the defect supercell with that in the bulk. $\mu[\text{Se}]_{min}$ represents lower limit potential of Se corresponding to the Se – poor (In – rich) limit potential. When calculating the E_f upon Se – rich (In – poor) conditions, upper limit potential of Se $\mu[\text{Se}]_{max} = \mu[\text{Se}]_{bulk}$ is used. $\mu[\text{In}]_{bulk}$ is the chemical potential of In in In crystal, and $E[In_2Se_3]$ formation energy for the perfect In_2Se_3. Based on the results in Fig.9, it is obvious that Li^+ prefers the interstitial site (Li_i^{1+}) for Se–rich condition. Besides, it is possible for Li to occupy Se (Li_{Se}^{2+}) or interstitial sites at low Fermi energy at Se–poor condition. However, Li ions preferentially occupy the interstitial sites as Fermi energy increases, and have the least possibility to occupy the In sites (Li_{In}^0).

Owing to the Li incorporation interstitially in – In_2Se_3, the lattice constants a and c show an increasing tendency, as indicates in Table 1, although a (7.337 Å) and c (19.71 Å) values from calculation are larger than those of experimental data (a: 7.056~7.090 Å; c: 19.30~19.35 Å). Besides, the a and c values for the case of Li substitution for Se is the smallest due to much smaller atomic radius of Li than that of Se. Therefore, the dominating occupation of Li should be in the interstitial sites, based on the variation of lattice constants a and c values.

Since the electronic level of Li^+ / Li is far above the Fermi level (F_r),[22] the occupied Li should remain ionized Li^+. Upon Li^+ incorporation in γ – In_2Se_3, F_r unpins and moves into the conduction band. The donor levels seems to merge with the conduction band, see Fig.10a and Fig.10b. Although the bandgap has a limited change, it is suggested that the incorporated Li ions, acting as a donor, must locate within the band structure of the host and are responsible for the enhancement in carrier concentration (Fig.4). Inset in Fig.10a is the unit cell

with Li occupation interstitially (here only one Li atom in the 2×2×1 unit cell is represented). After the movement of F_r into the CB, the effective mass of the conduction bands (CB) in both cases is very small if compared with that of VB, which further supports the remarkable improvement of the electrical conductivity (see Fig.5, and 6).

4. Conclusions

Lithiation ofvγ – In_2Se_3 powder has been conducted in the lithium acetate (CH_3COOLi) solution, and the band structure and TE properties of lithiated samples have been examined. Through the measurement of Hall coefficients, we have observed that the Hall carrier concentration (n_H) at RT is 1.71×10^{18} cm^{-3} after 30 h lithiation at 50 C°, increased by about 4 orders of magnitude compared to that of pristine γ – In_2Se_3. The highest electrical conductivities are 1.08×10^4 $\Omega^{-1}m^{-1}$ ($\sigma_{\perp}$) and 1.11×10^4 $\Omega^{-1}m^{-1}$ ($\sigma_{//}$) at ~923 K, about 40 times that of pristine γ – In_2Se_3 respectively. The first principle calculation reveals that Li^+ is energetically favorable to the interstitial sites in γ–In_2Se_3, and that the Fermi level (F_r) unpins and moves to the conduction band (CB). The modification in band structures directly elucidates the origin of the remarkable improvement of electrical conductivity. Along with the lowest lattice thermal conductivity (κ_L) of the sample, the highest ZT value of 0.62~0.67 was attained. This value is about 9~10 times that of pristine γ–In_2Se_3.

Supporting Information

The X-ray diffraction patterns of the lithiated γ–In_2Se_3; HRTEM images for the sample (lithiation: 30 h and 50 C°); TE performance parallel to the pressing direction ($C_{//}$); EPMA mapping of two elements In and Se on polished γ – In_2Se_3 surface; XRD pattern of the sample after measurement from high temperature to RT. The Supporting Information is available free of charge on the ACS Publications website at DOI: 10.1021/acs.chemmater.5b01389.

AUTHOR INFORMATION

Corresponding Author

* To whom correspondence should be addressed.
E–mail: cuijiaolin@163.com

Author Contributions

The manuscript was written through contributions of all authors. / All authors have given approval to the final version of the manuscript.

Notes

The authors declare no competing financial interest.

ACKNOWLEDGMENT

This work was supported by the National Natural Science Foundation of China (51671109, 51171084, 11604233), and Zhejiang Provincial Natural Science Foundation (LY14E010003, LQ14E010001).

ABBREVIATIONS

TE, thermoelectric; RT, room temperature; CB, Conducrion; VB: Valence band

REFERENCES

(1) Pei, Y.; Shi, X.; LaLonde, A.; Wang, H.; Chen, L.; Snyder, G. J. Convergence of Electronic Bands for High Performance Bulk Thermoelectrics. *Nature* **2011**, *473*, 66–69.

(2) Heremans, J. P.; Jovovic,V.; Toberer, E. S.; Saramat, A.; Kurosaki, K.; Charoenphakdee, A.; Yamanaka, S.; Snyder, G. J. Enhancement of Thermoelectric Efficiency in PbTe by Distortion of the Electronic Density of States. *Science* **2008**, *321*, 554–557.

(3) Zhao, L.; Tan, G.; Hao, S.; He, J.; Pei, Y.; Chi, H.; Wang, H.; Gong, S.; Xu, H.; Dravid, V. P.; Uher, C.; Snyder, G. J.; Wolverton, C.; Kanatzidis, M. G. Ultrahigh Power Factor

and Thermoelectric Performance in Hole-Doped Single–Crystal SnSe. *Science* **2016**, *351*, 141–144.

(4) Zhao, L.; Lo, S.; Zhang, Y.; Sun, H.; Tan, G.; Uher, C.; Wolverton, C.; Dravid, V. P.; Kanatzidis, M. G. Ultralow Thermal Conductivity and High Thermoelectric Figure of Merit in SnSe Crystals. *Nature* **2014**, *508*, 373–378.

(5) Polymeris, G. S.; Vlachos, N.; Khan, A. U.; Hatzikraniotis, E.; Lioutas, Ch. B.; Delimitis, A.; Pavlidou, E.; Paraskevopoulos, K. M.; Kyratsi, Th. Nanostructure and Doping Stimulated Phase Separation in High – ZT $Mg_2Si_{0.55}Sn_{0.4}Ge_{0.05}$ Compounds. *Acta Mater.* **2015**, *83*, 285–293.

(6) Pan, Y.; Li, J. Thermoelectric Performance Enhancement in N – type $Bi_2(TeSe)_3$ Alloys Owing To Nanoscale Inhomogeneity Combined With a Spark Plasma–Textured Microstructure. *NPG Asia Mater.* **2016**, *8*, e275.

(7) Watanabe, Y. C.; Kanako, S. C.; Kawazoe, H.; Yamane, M. Imperfections in Amorphous Chalcogenides. IV. A Model of Electrical Conduction Processes in Amorphous and Crystalline In_2Se_3. *Phys. Rev. B* **1989**, *40*, 3133–3142.

(8) Cui, J.; Liu, X.; Zhang, X.; Li, Y.; Deng, Y. Bandgap Reduction Responsible for the Improved Thermoelectric Performance of Bulk Polycrystalline $In_{2-x}Cu_xSe_3$ (x=0–0.2). *J. Appl. Phys.* **2011**, *110*, 023708.

(9) Cui, J.; Zhang, X. J.; Deng, Y.; Fu, H.; Yan, Y. M.; Gao, Y. L.; Li, Y. Y. Modified Structures and Improved Thermoelectric Property in Ag – Added Polycrystalline In_2Se_3. *Scripta. Mater.* **2011**, *64*, 510–512.

(10) Cui, J.; Wang, L.; Du, Z.; Ying, P.; Deng, Y. High Thermoelectric Performance of a Defect in α–In_2Se_3–Based Solid Solution upon Substitution of Zn for In. *J. Mater. Chem. C.* **2015**, *3*, 9069–9075.

(11) Likforman, A.; Foureroy, P. H.; Guittard, M.; Flahant, J.; Poirier, R.; Szydlo, N. Transitions de la Forme de Haute Température α de In_2Se_3, de part et d'autre de la Température Ambiante. *J. Solid State Chem.* **1980**, *33*, 91-97.

(12) Popović, S.; Tonejc, A.; Gržeta–Plenković, B.; Trojko, R. Revised and New Crystal Data for Indium Selenides. *J. Appl. Crystallogr.* **1979**, *12*, 416–420.

(13) Popović, S.; Čelustka, B.; Bidjin, D. X–Ray Diffraction Measurement of Lattice Parameters of In_2Se_3. *Phys. Stat. Sol. a* **1971**, *6*, 301–304.

(14) Eddike, D.; Ramdani, A.; Brun, G.; Tedenac, J. C.; Liautard, B. Phase Diagram Equilibria In_2Se_3–Sb_2Se_3 Crystal Growth of the β–Phase $In_{1.94}Sb_{0.06}Se_3$. *Mater. Res. Bull.* **1998**, *33*, 519–523.

(15) Landuyt, J. Van.; Tendeloo, G. Van.; Amelinckx, S. Phase Transitions in In_2Se_3 as Studied by Electron Microscopy and Electron Diffraction. *Phys. Stat. Sol. a* **1975** , *30*, 299–314.

(16) Marsillac, S.; Combot-Marie, A. M.; Bernède, J. C.; Conan, A. Experimental Evidence of the Low-Temperature Formation of γ-In_2Se_3 Thin Films Obtained by a Solid-State Reaction. *Thin Solid Films* **1996**, *288*, 14-20.

(17) Peng, H.; Zhang, X. F.; Twesten, R. D.; Cui, Y. Vacancy Ordering and Lithium Insertion in II_2VI_3 Nanowires. *Nano Res*. **2009**, *2*, 327–335.

(18) Pfitzner, A.; Lutz, H. D. Redetermination of the Crystal Structure of γ–In_2Se_3 by Twin Crystal X–ray Method. *J. Solid State Chem*. **1996**, *124*, 305–308.

(19) Ye, J.; Soeda, S.; Nakamura, Y.; Nittomo, O. Crystal Structure and Phase Transformation in In_2Se_3 Compound Semiconductor. *Jpn. J. Appl. Phys*. **1998**, *37*, 4264–4271.

(20) Julien, C.; Balkanski, M. Optical and Electrical Transport Studies in $Li_{0.1}In_2Se_3$. *Mater. Sci. Eng. B* **1996**, *38*, 1–8.

(21) Zhao, J.; Yang, L. Structure Evolutions and Metallic Transitions in In_2Se_3 Under High Pressure. *J. Phys. Chem. C* **2014**, *118*, 5445–5452.

(22) Julien, C.; Hatzikraniotis, E.; Chevy, A.; Kambas, K. Electrical Behavior of Lithium Intercalated Layered In – Se Compounds. *Mater. Res. Bull*. **1985**, *20*, 287–292.

(23) Julien, C.; Edurief, M.; Balkanski, M.; Hatzikraniotis, E.; K. Kambas, Electrical Transport Properties of In_2Se_3. *Phys. Stat. Sol. a* **1985**, *88*, 687–695.

(24) Yadav, A. A.; Salunke,S. D. Photoelectrochemical Properties of In_2Se_3 Thin Films: Effect of Substrate Temperature. *J. Alloys Compd*. **2015**, *640*, 534-539.

(25) Blöchl, P. E. Projector Augmented-Wave Method. *Phys. Rev. B: Condens. Matter Mater. Phys*. **1994**, *50*, 17953–17979.

(26) Perdew, J. P.; Burke, K.; Ernzerhof, M. Generalized Gradient Approximation Made Simple. *Phys. Rev. Lett*. **1996**, *77*, 3865–3868.

(27) Kim, H.; Gibbs, Z. M.; Tang, Y.; Wang, H.; Snyder, G. J. Characterization of Lorenz Number With Seebeck Coefficient Measurement. *APL Mater*. **2015**, *3*, 041506.

(28) Lutz, H. D.; Fischer, M.; Baldus, H. P.; Blachnik, R. Zur Polymorphie Des In_2Se_3. *J. Less Common. Met*. **1988**, *143*, 83-92.

(29) Chaiken, A.; Nauka, K.; Gibson, G. A.; Lee, H.; Yang, C. C.; Wu, J.; Ager, J. W.; Yu, K. M.; Walukiewicz, W. Structural and Electronic Properties of Amorphous and Polycrystalline In_2Se_3 Films. *J. Appl. Phys*. **2003**, *94*,

2390–2397.

(30) Yudasaka, M.; Matsuoka, T.; Nakanishi, K. Indium Selenide Film Formation by the Double-Source Evaporation of Indium and Selenium. *Thin Solid Films 1987*, **146**, 65-73.

(31) Pei, Y.; Lensch–Falk, J.; Toberer, E. S.; Medlin, D. L.; Snyder, G. J. High Thermoelectric Performance in PbTe Due to Large Nanoscale Ag_2Te Precipitates and La Doping. *Adv. Funct. Mater*. **2011**, *21*, 241–249.

(32) Lee, D. W.; Kingery, W. D. Radiation Energy Transfer and Thermal Conductivity of Ceramic Oxides. *J. Am. Ceram. Soc*. **1960,** *43*, 594–607.

(33) Pengelly, A. E. Heat Transfer Through Oxide-Cathode Materials. *Brit. J. Appl. Phys*. **1995**, *6*, 18–20.

(34) M. McQuarrie. Thermal Conductivity: VII, Analysis of Variation of Conductivity With Temperature for $A1_20_3$, BeO, and MgO. *J. Am. Ceram. Soc*. **1995**, *37* [2, Part II], 91–95.

(35) Charvat, F. R.; Kingery, W. D. Thermal Conductivity: XIII. Effect of Microstructure on Conductivity of Single – Phase Ceramics. *J. Am. Ceram. Soc*. **1957**, *40*, 306–315.

(36) Dubey, K. S.; Verma, G. S. Role of Peripheral Phonons in the Lattice Thermal Conductivity of Doped Semiconductors: Application to n-Ge. *Phys. Rev. B* **1971**, *4*, 2071–2074.

(37) Badir Khan, Z.K.; Dubey, K.S. Peripheral Phonons and Phonon Conductivity of a Metal at Low Temperatures. *Solid State Commun*. **1981**, *38*, 279-282.

(38) Xu, Y.; Li, Z.; Duan, W. Thermal and Thermoelectric Properties of Graphene. *Small* **2014**, *10*, 2182–2199.

(39) Rhyee, J. S.; Lee, K.H.; Lee, S.M.; Cho, E.; Kim, S.II.; Lee, E.; Kwon, Y.S.; Shim, J.H.; Kotliar, G. Peierls Distortion as a Route to High Thermoelectric Performance in $In_4Se_{3-\delta}$ Crystals. *Nature* **2009**, *459*, 965–968.

(40) Emziane, M.; Marsillac, S.; Bernède, J. C. Preparation of Highly Oriented $\alpha - In_2Se_3$ Thin Films by a Simple Technique. *Mater. Chem. Phys*. **2000**, *62*, 84–87.

(41) Julien, C.; Khelfa, J. A.; Benramdane, N.; Guesdon, J. P.; Dzwonkowski, P.; Samaras, I.; Balkanski, M. Lithium Insertion in Indium Selenide Films: Application to Microbatteries. *Mater. Sci. Eng. B* **1994**, *23*, 105–115.

(42) Balkanski, M.; Kambas, K.; Julien, C.; Hammerberg,J.; Schleich, D. Optical and Transport Measurements on Lithium $\alpha - In_2Se_3$ Layered Compounds. *Solid state Ionics* **1981**, *5*, 387–390.

(43) Balkanski, M.; Julien,C. *Insertion cathodes for solid state microbatteries, solid state microbatteries*; Ed: J. R. Akridge and M. Balkanski, Plenum Press, New York,

1990, 269–292.

(44) Han, G.; Chen, Z.; Drennan, J.; Zou, J. Indium Selenides: Structural Characteristics, Synthesis and Their Thermoelectric Performances. *Small* **2014**, *10*, 2747–2763.

Captions for figures

Fig.1 SAED pattern of a lithiated $\gamma-In_2Se_3$ powder (for lithiation 30 h at a fixed temperature of 50 C°). Inset: EDS spectrum, only In and Se elements are represented without Li signal. Cu peaks come from Cu grid.

Fig.2 (a) EEL spectrum of pristine γ–In_2Se_3 powder, inset is its TEM image, where a small peak around ~56 eV assigned to the Se core level; (b) Corresponding line spectrum of pristine $\gamma-In_2Se_3$ with background subtracted; (c) EEL spectrum of lithiated γ–In_2Se_3 powder with 30 h lithiation at 50 C°, inset is its TEM image; (d) Corresponding line spectrum of lithiated $\gamma-In_2Se_3$, where a large peak centered at ~56 eV, assigned to the Se mixed with Li core levels, was clearly observed.

Fig.3 The lattice constants *a* and *c* as a function of lithiation time (at a fixed lithiation temperature of 50 C°) (a), and lithiation temperature (for a fixed lithiation time of 30 h) (b), upon Li diffusion into the γ–In_2Se_3.

Fig.4 Measured Hall carrier concentration (n_H) and mobility (μ) of the lithiated $\gamma-In_2Se_3$ at a fixed lithiation temperature of 50 C° (a), and for a fixed lithiation time of 30 h (b).

Fig.5 The thermoelectric properties of lithiated $\gamma-In_2Se_3$ ($C_\perp$) as a function of lithiation temperature for the fixed lithiation time of 30 h. (a) Seebeck coefficient (α), (b) Electrical conductivity (σ), (c) Lattice thermal conductivity (κ_L), insert is the total thermal conductivity (κ), (d) ZT value.

Fig.6 The thermoelectric properties of lithiated $\gamma-In_2Se_3$ ($C_\perp$) as a function of lithiation time at a fixed lithiation temperature of 50 C°. (a) Seebeck coefficient (α), (b) Electrical conductivity (σ), (c) Lattice thermal conductivity (κ_L), insert is the total thermal conductivity (κ), (d) ZT value.

Fig.7 Measured thermoelectric properties of the sample ($C_{//}$, lithiation 30 h at 50 C°) in heating cycle (▼) and cooling cycle (○). (a) Electrical conductivity (σ), (b) Seebeck coefficient (α), (c) Total thermal conductivity (κ), an inset is the lattice contribution (κ_L), (d) ZT value.

Fig.8 (a) Band structure (left) and the density of states (DOS) (right) of $\gamma-In_2Se_3$. (b) 3D electron localization function (ELF) isosurfaces maps of $\gamma-In_2Se_3$ for ELF=0.8 (left) and ELF=0.9 (right). ELF = 1 corresponding to perfect localization and ELF = ½ corresponding to the

electron gas. The ELF of γ−In_2Se_3 shows a lobe−shaped asymmetrically localized electron cloud around Se^{2-}, indicating the degree of electron localization.

Fig.9 Formation energies (E_f) of defects as a function of the Fermi energy (F_f) under the Se−rich and Se−poor conditions.

Fig.10 (a) The band structure of Li interstitially occupied γ−In_2Se_3, an inset is the relaxed structure of Li interstitially occupied γ−In_2Se_3 (here only one Li atom in the 2×2×1 unit cell is represented, the dotted circled is the interstitial Li atom); (b) The band structure of Li occupying the Se sites. In both cases, the Fermi level (F_f) unpins and moves into the conduction band (CB).

Table captions

Table 1 The relaxed lattice constant of perfect bulk γ−In_2Se_3, Li interstitial, Li substitution for Se and In.

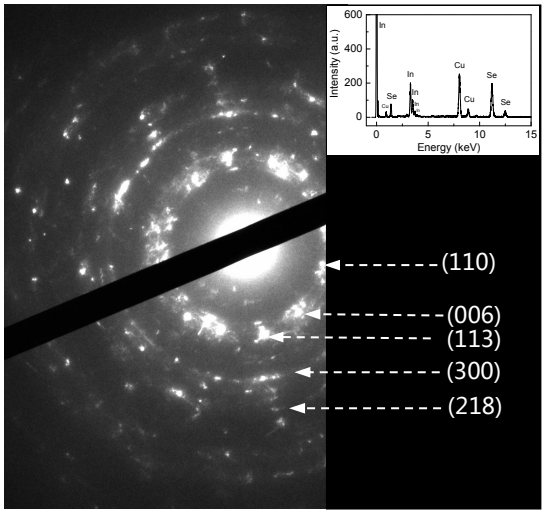

Figure 1

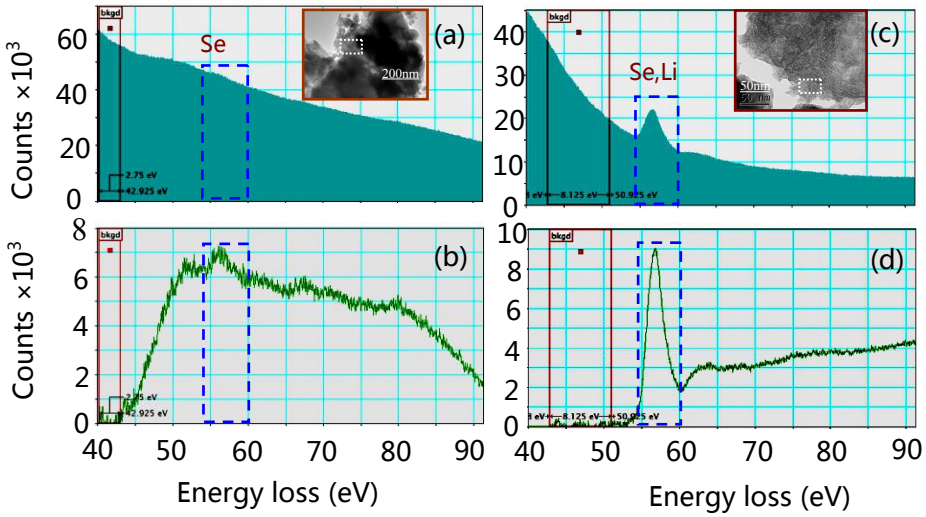

Figure 2

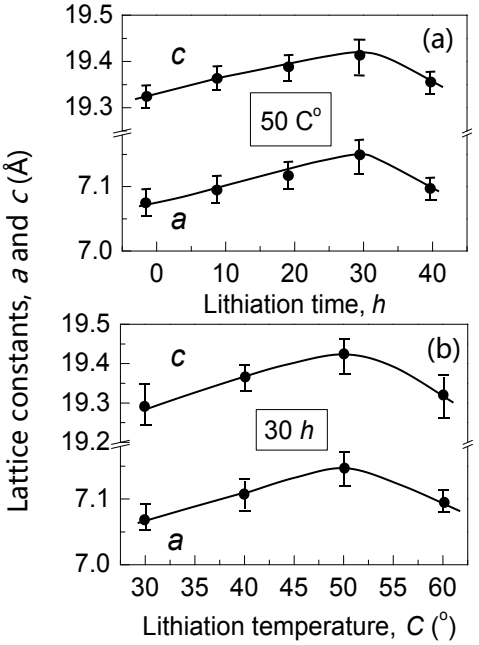

Figure 3

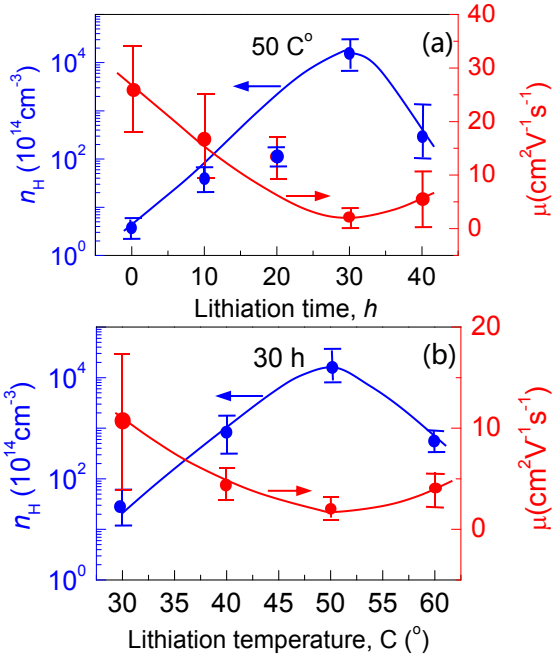

Figure 4

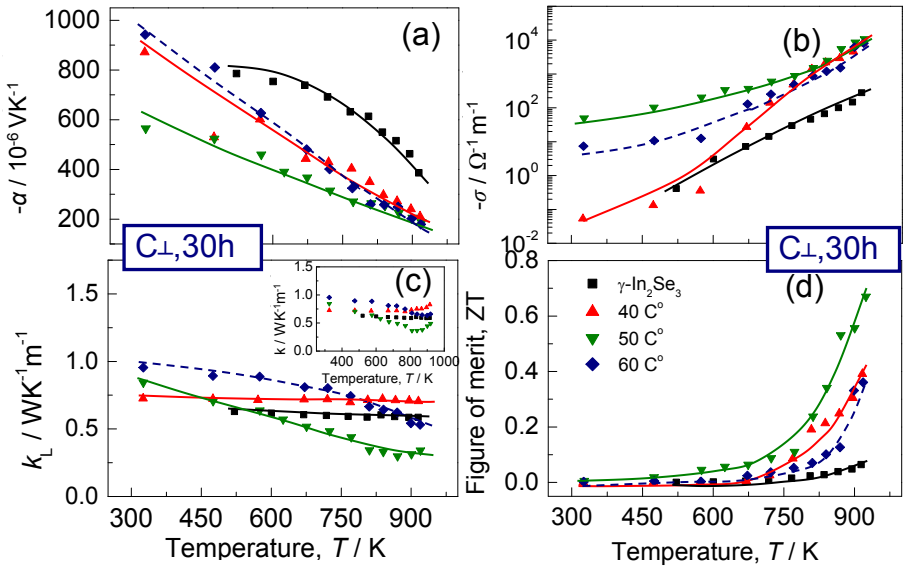

Figure 5

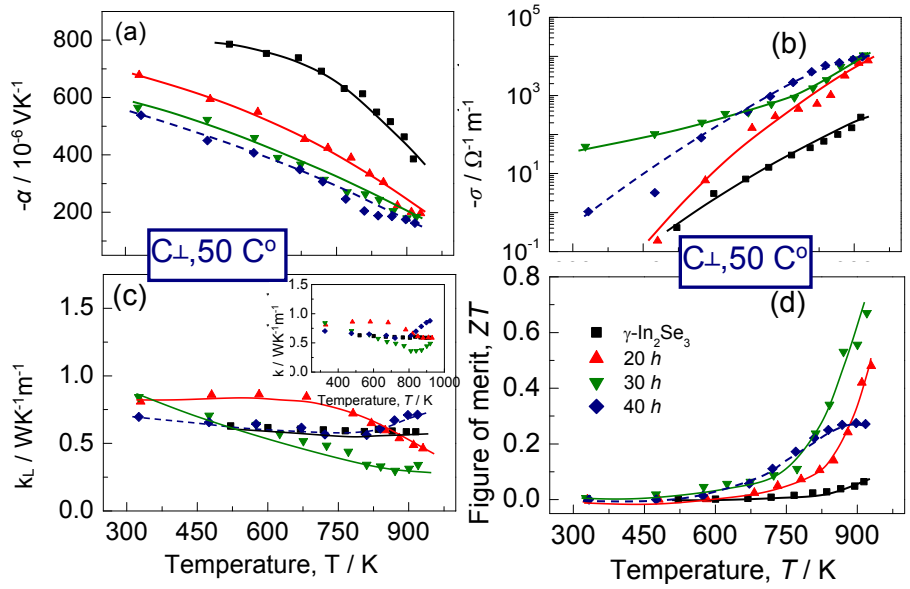

Figure 6

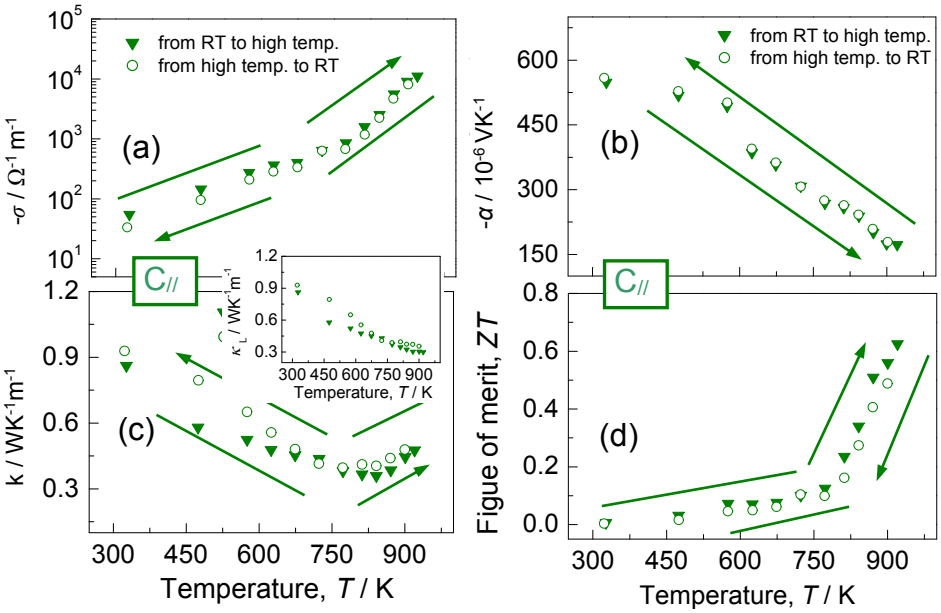

Figure 7

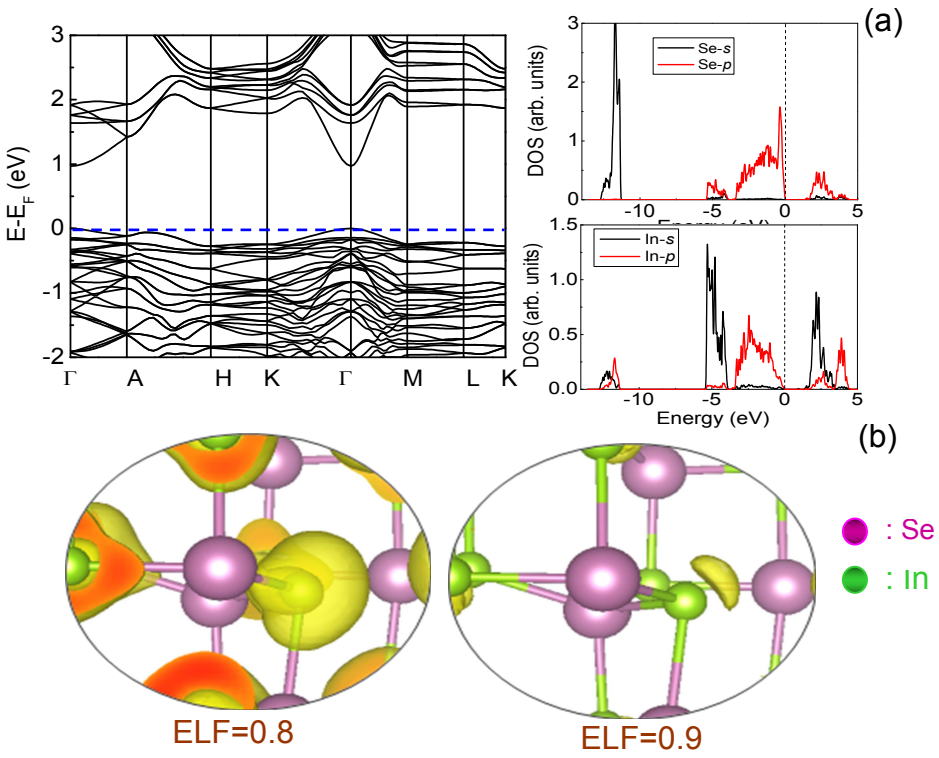

Figure 8

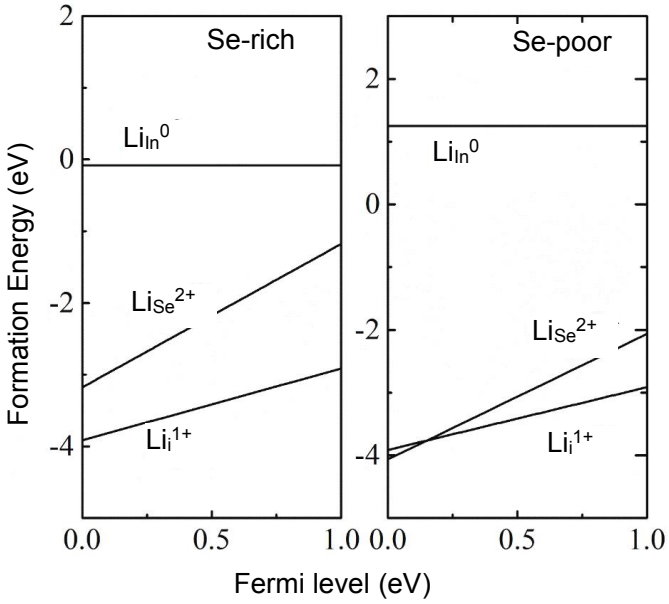

Figure 9

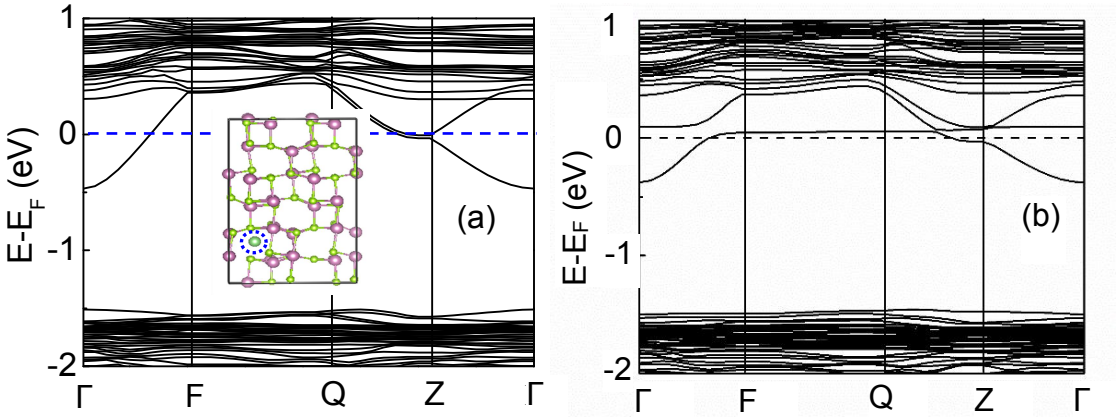

Figure 10

Table 1

	γ-In_2Se_3	Li_i	Li_{Se}	Li_{In}
a (Å)	7.337	7.426	7.326	7.399
c (Å)	19.705	19.925	19.657	19.751

The table of contents entry